

Sampling Strategies to Optimize Coincident Remote Sensing and In Situ Cloud and Precipitation Observations from Multiple Aircraft

John E. Yorks^a,[✉] Matthew A. Miller,^b Timothy J. Lang,^c Joseph A. Finlon,^{a,d}
Ian S. Adams,^a Brian A. Colle,^e Steven J. Greybush,^f Andrew J. Heymsfield,^g
Gerald M. Heymsfield,^a Rachael Kroodsma,^a Samuel LeBlanc,^h
Matthew Walker McLinden,^a Greg M. McFarquhar,ⁱ Robert M. Rauber,^j
Sandra E. Yuter,^b Troy Zaremba,^k and Lynn A. McMurdie^k

KEYWORDS:

Clouds;
Mesoscale
processes;
Snowbands;
Precipitation;
Synoptic-scale
processes;
Aircraft
observations

ABSTRACT: The combination of simultaneous, collocated aircraft in situ measurements and remote sensing data at multiple wavelengths is of tremendous value in physical process studies but is hard to obtain in practice. Appropriate multi-aircraft and multisensor resources for a given project must be coupled with agile mission support (people and tools) and close coordination with the Federal Aviation Administration to implement successfully. Obtaining closely coordinated in situ and remote sensing measurements was key to meeting the science objectives for the NASA Investigation of Microphysics and Precipitation for Atlantic Coast-Threatening Snowstorms (IMPACTS), and it required a team effort. IMPACTS flew a complementary suite of remote sensing and in situ instruments in three 6-week deployments on the NASA ER-2 and P-3 aircraft to provide observations critical to understanding the mechanisms of snowband formation, organization, and evolution. The collocated IMPACTS data subset encompassed 106 flight legs during 22 storms, and it included over 21 h where the ER-2 and P-3 were only up to 5 min and 4 km apart. This unique dataset on winter storm conditions in the Northeast and Midwest United States provides a wealth of information, which will have lasting value for the community. This paper explains how the science team, engineers, aircrews, and NASA mission support accomplished the measurement goals and key aspects of the IMPACTS coordinated dataset. Future field campaigns with similar science applications can maximize their flight hours by leveraging the lessons learned from IMPACTS coordination.

SIGNIFICANCE STATEMENT: Winter storms feature poorly understood and predicted snowbands where precipitation is concentrated. NASA funded a multiyear field campaign using complementary aircraft to study these bands over the United States. The project employed two aircraft in a stacked configuration: one plane flew within storms, similar to Hurricane Hunters, using cloud probes to collect in situ measurements, while the other plane flew above with advanced radars and other instruments to simulate satellite observations. By flying coordinated patterns perpendicular to snowbands, the project collected 21 h of collocated data of ice crystals and storm structure. This data will improve both space-based snowfall measurement capabilities and model-based snowfall forecasts through enhanced understanding of the complex processes within winter storms.

DOI: 10.1175/BAMS-D-24-0280.1

Corresponding author: John E. Yorks, john.e.yorks@nasa.gov

Manuscript received 7 October 2024, in final form 1 October 2025, accepted 9 October 2025

© 2025 American Meteorological Society. This published article is licensed under the terms of the default AMS reuse license. For information regarding reuse of this content and general copyright information, consult the AMS Copyright Policy (www.ametsoc.org/PUBSReuseLicenses).

AFFILIATIONS: ^a NASA Goddard Space Flight Center, Greenbelt, Maryland; ^b Department of Marine, Earth, and Atmospheric Sciences, North Carolina State University, Raleigh, North Carolina; ^c NASA Marshall Space Flight Center, Huntsville, Alabama; ^d Earth System Science Interdisciplinary Center, College Park, Maryland; ^e School of Marine and Atmospheric Sciences, Stony Brook University, State University of New York, Stony Brook, New York; ^f Department of Meteorology and Atmospheric Science, The Pennsylvania State University, University Park, Pennsylvania; ^g NSF National Center for Atmospheric Research, Boulder, Colorado; ^h Bay Area Environmental Research Institute, NASA Ames Research Center, Mountain View, California; ⁱ School of Meteorology and Cooperative Institute for Severe and High Impact Weather Research and Operations, University of Oklahoma, Norman, Oklahoma; ^j Department of Climate, Meteorology, and Atmospheric Sciences, University of Illinois Urbana–Champaign, Urbana, Illinois; ^k Department of Atmospheric and Climate Science, University of Washington, Seattle, Washington

1. Introduction

Winter snowstorms disrupt transportation, commerce, and public safety, while their mesoscale precipitation variability presents significant challenges for operational weather forecasting. Substantial precipitation forecast errors result from relatively small spatial errors in rain–snow boundaries and snowband locations (Zhang et al. 2002; Ganetis and Colle 2015; Greybush et al. 2017), while remote sensing retrievals often assume uniform particle types despite ground and airborne measurements revealing complex mixtures of ice particle habits and rime fraction (Stark et al. 2013; Finlon et al. 2016). Major knowledge gaps exist regarding snowband initiation, organization, vertical structure, microphysical properties, and their representation in numerical models. Understanding the complex interactions between flow structure, thermodynamics, and microphysical processes across convective, mesoscale, and synoptic scales remains critical for predicting the spatial and temporal variability of precipitation within extratropical cyclones (Ralph et al. 2005). However, past observations and simulations of these interactions have not achieved adequate temporal and spatial resolution to diagnose particle growth processes within these storms (Hashino 2007). High-resolution collocated remote sensing and in situ observations of the vertical structure of snowbands and retrieved microphysical properties (Plummer et al. 2014, 2015; Finlon et al. 2016; Grecu et al. 2016, 2018), in conjunction with numerical models, are needed to assess the relative performance of different microphysical parameterizations (Han et al. 2010, 2013, 2018; Putnam et al. 2017) and improve these microphysical schemes.

Several field campaigns over the past 30 years have collected high-resolution remote sensing and in situ observations of precipitation structure and cloud microphysical properties, with varying success at collocating the datasets. Early field campaigns were able to colocate two aircraft that fly at similar speeds using preplanned flight patterns. For example, the Convection and Moisture Experiment (CAMEX-3) in 1998 collocated the NASA DC-8 and ER-2 within 3 km and 5 min for over 19 h based on aircraft navigation data (Kakar et al. 2006). In the Central Equatorial Pacific Experiment (CEPEX) in 1993 (Central Equatorial Pacific Experiment Design Document 1993), collocation between the Aeromet Learjet and NASA ER-2, as well as with the NOAA P-3, was attempted but complicated by different speeds of the aircraft. However, in both experiments, there were no capabilities to monitor instrument health or changes in targeted weather phenomena in real time, making it difficult to ensure the collocated data of the targeted phenomenon were captured.

Starting in the late 2000s, real-time downlinking of instrument and weather data became possible through tools like NASA's Real-Time Mission Monitor (RTMM; Blakeslee et al. 2007) and later the Mission Tools Suite (MTS; Airborne Science Program 2025). However, budget constraints often limited field campaigns to a single aircraft or required different agencies or programs to fund participation by additional aircraft. For example, the Olympic Mountains Experiment (OLYMPEX), flown concurrently with the Radar Definition Experiment (RADEX) in late 2015, included the NASA DC-8, the ER-2, and the University of North Dakota (UND) Citation but was funded by multiple NASA programs, limiting the coordination (within 5 km and 5 min) between the aircraft to a total of roughly 31 min (Houze et al. 2017). Even when multiple aircraft were funded by the same program, such as the NASA ER-2 and P-3 during the 2016 Observations of Aerosols above Clouds and their Interactions (ORACLES) campaign, close coordination (e.g., Redemann et al. 2021) was defined to mean sampling the same cloud at different altitudes at the same time, rather than exact coordinated flying. Recent NASA projects, with more robust budgets, have been able to collocate multiple aircraft with more success, such as the Aerosol Cloud Meteorology Interactions over the Western Atlantic Experiment (ACTIVATE) that collected 278.5 h of collocated data to within 6 km and 5 min during six deployments from February 2020 to June 2022 (Schlosser et al. 2024), but had science objectives focused on small-scale cloud and aerosol interactions that do not meet the needs of the winter precipitation community.

The Investigation of Microphysics and Precipitation for Atlantic Coast-Threatening Snowstorms (IMPACTS) flew a complementary suite of remote sensing and in situ instruments in three 6-week deployments on the NASA ER-2 and P-3 aircraft to provide observations critical to understanding the mechanisms of snowband formation, organization, and evolution (McMurdie et al. 2022). Deployments were conducted in 2020, 2022, and 2023 during the months of January and February (a planned 2021 deployment was delayed due to COVID). The NASA P-3 aircraft deployed from the Wallops Flight Facility in Wallops Island, Virginia, its headquarters, minimizing costs and logistical issues. To reduce the impact of adverse winter weather on operations, the NASA ER-2 aircraft was based out of the Southeast United States but changed each year due to hangar availability: Hunter Army Airfield (Savannah, Georgia) in 2020, Pope Army Airfield (Fayetteville, North Carolina) in 2022, and Dobbins Air Reserve Base (Marietta, Georgia) in 2023. During these three deployments, IMPACTS conducted a total of 35 science flights (total flights, coordinated and uncoordinated), 26 ER-2 flights for 218 h, and 33 P-3 flights for 267 h during a variety of winter storms.

IMPACTS scientists employed a three-level sampling strategy to observe winter storms and achieve its science objectives. The NASA ER-2 aircraft served as an advanced cloud and precipitation remote sensing platform capable of simulating satellite sensors from above the clouds and precipitation, but with advanced measurement capabilities (multifrequency, nadir-viewing radars) and much higher spatial and temporal resolution. The P-3 served as the IMPACTS in situ platform at storm level for identifying microphysical particle characteristics, the local environment of the particles, and vertical thermodynamic and kinematic profiles from dropsondes. On the ground, mobile radar systems and radiosondes provided additional large-scale perspectives of the thermodynamic environments and storm system structures. We present in this paper the strategies utilized by the IMPACTS team to coordinate the two aircraft, including the five-point flight legs that enabled the collection of a robust collocated remote sensing and in situ (microphysical and thermodynamic) dataset that is critical to improving snowfall retrieval algorithms and numerical weather prediction microphysics schemes.

2. IMPACTS aircraft and sensors

a. Aircraft. The NASA ER-2's range, altitude, and real-time data downlinking capabilities made it ideally suited to provide the remote sensing measurements required for IMPACTS.

TABLE 1. Aircraft specifications of relevance for IMPACTS collocation.

Parameter	ER-2	P-3
Cruise altitude	20 km	0.5–6.7 km
Cruise speed	210 m s ⁻¹	144–175 m s ⁻¹
Range	>5000 km	7000 km
Endurance	7–8 h	10 h
IMPACTS location	Southeast United States	Wallops Island, Virginia

The nominal altitude, speed, range, endurance, and IMPACTS base locations for both aircraft are provided in Table 1. For IMPACTS, the ER-2 flew above cloud systems at ~65 000 ft (20 km), carrying radars, a lidar, radiometers, and electric field meters that have a long history of flying on the aircraft. The NASA P-3 is designed for low-altitude heavy-payload applications, making it ideal for the IMPACTS suite of in situ instrumentation. The P-3 nominal altitude, speed, range, endurance, and IMPACTS base location are reported in Table 1. The vertical range of the P-3 with the IMPACTS payload configuration varied from 300 ft (90 m) over water (conditions permitting) up to 22 000 ft (6.7 km), ensuring the full vertical sampling of cloud and precipitation structures. During IMPACTS, the typical freezing altitude of the storms sampled was often below the ground (12 out of 21 coordinated flights) but occasionally was as high as 3 km. During the latter scenario, the P-3 typically flew lower-altitude legs (below 3 km) at temperatures above freezing last, to mitigate in situ probe icing.

b. Remote sensing. A total of eight remote sensing instruments flew on the ER-2 during IMPACTS, providing the vertical and horizontal structure of storms. Key specifications of each instrument are provided in Table 2. Three radars flew on the ER-2: the Cloud Radar System (CRS), High Altitude Wind and Airborne Profiler (HIWRAP), and ER-2 Doppler Radar (EXRAD). All three radars measure the reflectivity and radial velocity of precipitation and clouds with nadir-looking beams (Li et al. 2016; Walker McLinden et al. 2021;

TABLE 2. Key specifications of the IMPACTS remote sensing instruments.

Instrument	Frequency or wavelength	Resolutions/swath	Other specifications
CRS	W band (94 GHz)	Horizontal: 200 m Vertical: 115 m	Nadir pointing; 50-m horizontal sampling; vertical sampling: 14 m
HIWRAP	Ku band (14 GHz) Ka band (35 GHz)	Horizontal (Ku): 800 m Horizontal (Ka): 350 m Vertical: 130 m	Nadir pointing; 100-m horizontal sampling; vertical sampling: 26 m
EXRAD	X band (9.6 GHz)	Horizontal: 1 km Vertical: 150 m	Nadir pointing; 100-m horizontal sampling; vertical sampling: 13 m; additional conical scanning beam with ~30° tilt angle (20 km swath width)
CPL	355, 532, 1064 nm	Horizontal: 200 m Vertical: 30 m	Depolarization ratio at 1064 nm; nadir pointing
AMPR	10.7, 19.35, 37.1, 85.5 GHz	Swath width: 38 km IFOV: 0.6–2.8 km	Cross-track scanning; dual polarized; four scene sweeps and calibration sequence (10–12 s)
CoSMIR	50.3, 52.8, 89.0, 165.5, 183.31 GHz	Swath width: 50–60 km Res: 1.4–3.9 km	New scan configurations in 2020; conical/along-track scan in 2022
CoSSIR	170.5, 183.31, 325.15, 684.0 GHz	Swath width: 50–60 km Res: 1.4–3.9 km	Used in 2023 deployment only; conical/along-track scan
LIP	—	50-Hz sampling rate	Dynamic range: ~10 ⁰ –10 ⁶ V m ⁻¹ ; ~10% measurement error

Heymsfield et al. 2023). The fine-scale spatial sampling of the IMPACTS airborne radars, 100 m in the horizontal and ~ 10 m in the vertical, provides a much more detailed view of the storm structures than NWS radars, which typically have spatial scales of several hundreds of meters to several kilometers depending on range from the radar. The Cloud Physics Lidar (CPL) is a nadir-pointing, multiwavelength elastic backscatter lidar that measures vertical profiles of cloud and aerosol properties (McGill et al. 2002). Depolarization ratio estimates, which provide information about particle sphericity (Yorks et al. 2011b), are provided at 1064 nm. IMPACTS flew three different microwave radiometers, two at a given time, during the three deployments to provide brightness temperatures. The Advanced Microwave Precipitation Radiometer (AMPR; Amiot et al. 2021; Richter and Lang 2024) is a four-frequency, dual-polarized, cross-track-scanning microwave radiometer with a 38-km swath. The Conical Scanning Millimeter-Wave Imaging Radiometer (CoSMIR) and the Configurable Scanning Submillimeter-Wave Instrument/Radiometer (CoSSIR) are a pair of microwave radiometers that share a common configurable scanning architecture (Kroodsmas et al. 2019; Liu and Adams 2025). During the first deployment of IMPACTS (2020), CoSMIR was flown in two new configurations—forward/aft conical and conical/along track (50–60-km swath). The latter scan strategy was adopted for the 2022 (CoSMIR) and 2023 (CoSSIR) deployments to provide important horizontal context to the snowstorms in a conical scan geometry similar to the Global Precipitation Measurement (GPM) Microwave Imager (GMI) and enable along-track observations for the development of high-vertical-resolution tomography algorithms (Liu and Adams 2025). The Lightning Instrument Package (LIP) flew on the ER-2 during all three IMPACTS campaigns (Schultz et al. 2021). Three-dimensional (3D) electric field vectors are retrieved as well as electric field changes due to lightning.

c. *In situ* sensors. IMPACTS employed several different cloud probes to provide redundancy across a wide particle size range, as shown in Fig. 1. The Cloud Droplet Probe (CDP) and Fast CDP (FCDP) use forward-scattering principles to measure the size distributions of cloud water droplets. The Particle Habit Imaging and Polar Scattering (PHIPS) combines a high-resolution stereo-microscopic imager and a single-particle polar nephelometer to determine cloud particle shape, size, and habit using a $3\text{ mm} \times 2\text{ mm}$ field of view (Abdelmonem et al. 2016; Schnaiter et al. 2018; Waitz et al. 2021). For cloud droplets and larger ice particles, IMPACTS relied on the Two-Dimensional Stereo (2D-S) and two High-Volume Precipitation Spectrometer (HVPS-3) imaging probes oriented orthogonally. The Hawkeye probe, consisting of an FCDP, 2D-S, and Cloud Particle Imager (CPI), was impacted by shattering during IMPACTS but provided redundancy for comparative purposes. Cloud liquid content was measured

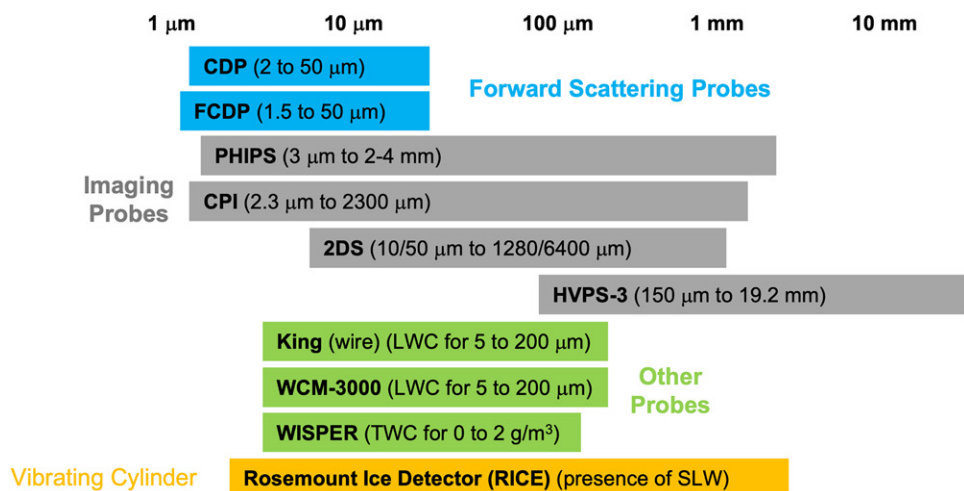


FIG. 1. Hydrometeor size ranges as measured by the IMPACTS cloud probes.

with a King Probe and Science Engineering Associates Model WCM-3000. IMPACTS also included a Rosemount Ice Detector (RICE) to detect the occurrence and amount of supercooled water. The Water Isotope System for Precipitation and Entrainment Research (WISPER) provided high-accuracy measurements of total water content that is the sum of liquid and ice content (Twohy et al. 1997). The Turbulent Air Motion Measurement System (TAMMS) instrument measures 3D winds, humidity, and temperature at the P-3 flight level (Brown et al. 1983). Derived measurements of the 3D wind components, temperature, and moisture are computed from the raw 100-Hz data and archived at 20-Hz resolution. The Diode Laser Hygrometer (DLH; Podolske et al. 2003), flown during the 2023 deployment, is a laser-based hygrometer that measures water vapor via differential absorption techniques at isolated spectral lines near 1.4 μm . While the in situ probes all have varying raw collection rates, data products are reported at 1 Hz for all sensors.

3. Collocation challenges

One of the biggest challenges of collocating the NASA ER-2 and P-3 was the differences in the cruise speeds of the two aircraft (Table 1), which were further exacerbated by the variations in the P-3 cruise speed based on altitude and winds. Figure 2 shows the variation of the ground-speed ratio (ER-2 to P-3) with the P-3 altitude for 2020 Fig. 2a, which was used to determine the optimal flight patterns in the last two deployments, and for all three deployments, Fig 2b. When the P-3 flew at higher altitudes (4–8 km), the ground speed ratio was typically 1.0–1.2, meaning the two aircraft were flying nearly the same cruise speeds. However, the ground-speed ratio was greater than 1.4 when the P-3 flew below 4 km in altitude. The differences in cruise speeds also necessitated longer legs and longer turns between legs for the ER-2 compared to the P-3, which reduced the amount of coincidental sampling time. Furthermore, the lower altitude of the P-3 required timely and accurate communication with local air traffic control (ATC) centers. If the P-3 flight plans were altered in real time during flight, or the aircraft was flying near a busy airport (New York, Chicago, etc.) or ATC was busy with other aircraft, delays to the P-3 led to further delays to the ER-2. Given that IMPACTS flights took place at various times of the day, targeting the timing of the predicted peak snowfall, this issue was exacerbated when flying during the busiest air traffic periods.

The heterogeneity of winter storms also led to challenges in coordinating the IMPACTS aircraft. Numerical weather prediction models can have errors in the forecast of the rain–snow lines or locations of snowbands on the order of tens to hundreds of kilometers (Zhang et al.

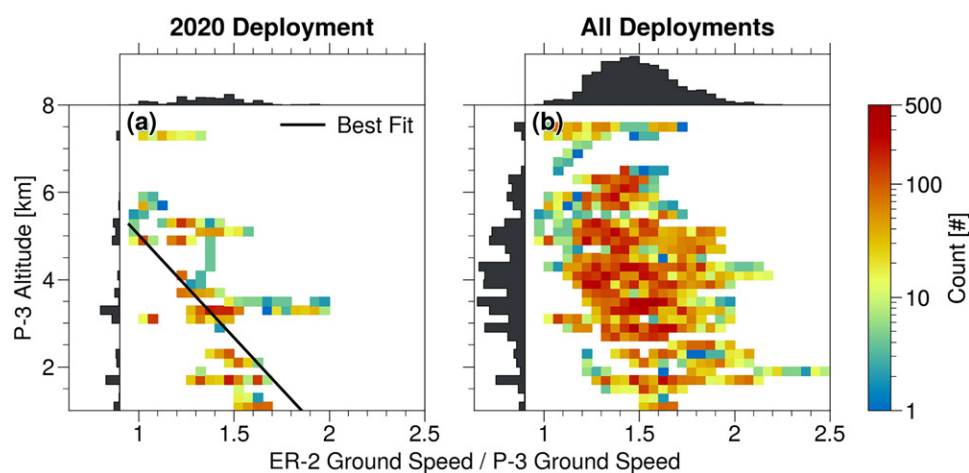


FIG. 2. The ground speed ratio (ER-2/P-3) vs P-3 altitude for (a) the 2020 deployment and (b) all deployments. Histograms of the P-3 altitudes are provided on the left side of the plots, while histograms of the ground speed ratio are provided on the top. A best-fit line in 2020 shows the origin of the ground speed ratios for the coordinated legs.

2002; Ganetis and Colle 2015; Greybush et al. 2017), which made planning the exact location of flight lines difficult 24–48 h before the storm. Even when models properly predict the locations of the snowbands, these bands typically evolve and move through the region of interest quickly during an 8-h flight, necessitating adjustments to the planned flight patterns. The evolution of these snowbands occurs rapidly (on the order of minutes in some cases), further challenging multi-aircraft coordination. Finally, vertical variations in horizontal wind speeds as the P-3 flies through frontal boundaries further introduce variability in the true ground speed of the P-3 compared to planned flight patterns, especially at lower altitudes. Another weather-related challenge to planning coordinated flights was the local weather conditions for takeoff and landing, which sometimes caused takeoff delays or an early return to base if landing conditions were forecast to deteriorate.

Instrument sampling rates and measurement volumes of the remote sensors also impact the ability to collocate the remote sensing and in situ data, even when the aircraft themselves are well coordinated. For example, the CPL points nadir and has a 100-microradian field of view, providing a narrow ~2-m diameter footprint at the altitude where many IMPACTS cloud tops were sampled (Yorks et al. 2011a). Additionally, cloud vertical profiles are limited to optical depths less than 3.0, causing CPL to only penetrate roughly 1–3 km deep into the cloud systems observed during IMPACTS. Thus, to collocate the in situ sensors with the lidar data without assumptions of particle homogeneity across large spatial scales, the P-3 must be flying near cloud top and within meters horizontally of this small lidar sampling “volume.” The collocation constraints for the high-altitude radars are less stringent, as the HIWRAP and EXRAD sensors have a footprint diameter of ~1 km. While these radars are sensitive to hydrometeors through most of the cloud depth, they are sometimes insensitive to small particles at the cloud tops that the lidars are sensitive to, which must be considered when flying the P-3 near cloud top. Attenuation in moderate to heavy rain can also occur at lower altitudes, particularly for higher-frequency radars like HIWRAP and CRS. Collocation between the microwave radiometers is simple in the horizontal direction, given the wide swaths of these sensors, but can be a challenge vertically if the instrument does not have a frequency sensitive to the cloud vertical structure at the P-3 altitude. Given that most of the remote sensors and in situ instruments report their data at 1 Hz, there are minimal sampling issues related to data rates.

4. Sampling strategies employed during IMPACTS

a. Separation requirements. Ice processes occurring at higher altitudes, such as riming, influence a significant portion of global precipitation patterns (Heymsfield et al. 2020). Although these mechanisms can enhance ice water content (IWC) within midlatitude storm systems (Waitz et al. 2021), researchers have not yet fully determined their quantitative impact on surface snowfall accumulation. Deng et al. (2024) suggest that small-scale ice clusters, areas of several kilometers exhibiting elevated ice particle concentrations or IWC, are primarily responsible for the nonuniform distribution of ice within cloud formations. Horizontal winds within the storm, often $>20 \text{ m s}^{-1}$ or more at altitudes greater than 4 km (20 m s^{-1} yields 6-km horizontal motion in 5 min), transport hydrometeors sideways an order of magnitude faster than they fall (Finlon et al. 2022; Tomkins et al. 2025). To observe these variations in cloud microphysical properties and transport over small spatial and temporal scales, the IMPACTS project defined a minimum collocation requirement for the two aircraft of 4 km horizontal separation and 5 min temporal separation. Several recent publications have used 3–5 min as a collocation threshold when using the combined remote sensing and in situ IMPACTS dataset (e.g., Finlon et al. 2022; Maherndl et al. 2024; Allen et al. 2025). Field campaigns that target other atmospheric applications may not require as stringent collocation temporal and spatial scales.

b. The five-point flight legs.

Figure 3 became the standard IMPACTS flight pattern later in 2020 operations due to the ease of the design, the effectiveness for coordinating aircraft timing, and the reduction in confusion when retasking one or both aircraft was required midflight. It uses two points to define the P-3 flight leg beginning and end (P1 and P2 in Fig. 3) and two

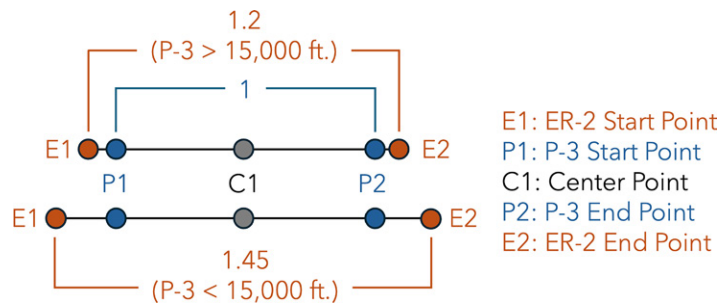


FIG. 3. The general five-point line concept for ground speed ratios of 1.2 (P-3 high altitudes) and 1.45 (P-3 low altitudes), with the aircraft start/end point labels.

points to define the ER-2 flight leg beginning and end (E1 and E2), based on the typical ground speed ratios of the two aircraft. The fifth center point (C1), where the aircraft are intended to overfly the same ground point at the same time, acts as a reference point for both aircraft to communicate estimated overflight times and coordinate changes in speed or turning locations to maintain close timing. The lines were initially planned based on the forecasted conditions for the first pass. However, as the P-3 would repeat passes at lower altitudes, the slower P-3 airspeeds at these altitudes and the vertical variations of the horizontal winds limited the collocation success and instrument collection, so delay maneuvers were performed by one or both aircraft to accommodate the 5-min collocation goal.

Initially, a P-3 to ER-2 leg length ratio of 1:1.2 led to coordination issues when the P-3 was flying slower than planned at lower altitudes. The ER-2 would overtake the P-3 before the center point, forcing it to ad lib leg extensions to maintain coordination, wasting sampling time. Flying shorter flight legs improved the temporal coordination between the airplanes. However, shorter lines required relatively more time turning around at the end of each line, reducing data collection time for many of the remote sensors, which require straight and level flight. The line lengths were sometimes adjusted during flights based on the width of the snowbands or features being sampled. By the 2023 deployment, the sampling strategy changed to using two 5-point flight lines during planning: a high-altitude line that used a leg length ratio of 1.20 and a low-altitude line that used a ratio of 1.45 (Fig. 3). Model initialization winds at the P-3 flight level were also used to estimate the influence of crosswind/headwind for the P-3 and gauge additional reductions in aircraft true airspeed, both during planning as well as during flights.

c. Moving lines software. The time and effort scientists spend planning flight paths according to science objectives, aircraft performance, airspace availability, meteorological and sampling conditions, airborne instruments needs, and coordination with other airborne research platforms can distract from accomplishing the science objectives. To mitigate this issue, a publicly available research flight planning tool called Moving Lines (LeBlanc 2018) was used and subsequently modified during IMPACTS. This flight planning tool focuses on building airborne sampling strategies for better resolving the environment surrounding aerosol, clouds, radiation, and atmospheric dynamics. To date, Moving Lines has been used during at least 10 NASA field campaigns including IMPACTS. It was built as an open-source Python library with a graphical user interface portraying mapping (Cartopy) and interfaces through simple spreadsheets (Excel). The fundamental interface is one spreadsheet tab per desired flight path, often used as different aircraft, like the NASA ER-2 and the P-3 used during IMPACTS, for planning coordinated science observations. This interface includes multiple waypoints for identifying latitudes and longitudes of sampling in concert with the vertical aircraft location.

Moving Lines, which can be configured for any field campaign, incorporates a parameterized set of aircraft characteristics, like typical cruise speed, altitude, turn bank angles, flight speed as a function of altitude, and climb rate for the different research aircraft in addition to solar geometry calculations, satellite overpass predictions, common flight modules, model/satellite imagery overplotting, and multiple aircraft plans. It also expands with predetermined flight sampling modules, for which many were custom designed for IMPACTS, like the five-point line for coordinated ER-2 and P-3 sampling (Fig. 4). As part of the design and building of the flight plans, Moving Lines calculates the flight time from the parameterized aircraft specifications and sampling design and can output pilot-friendly files for easier dissemination, as well as a multitude of figures and summary presentations for scientific feedback.

d. The primary benefit of the five-point-line scheme is the ease of use and planning. An IMPACTS flight leg was typically on the order of 150–250 km or 15–25 min of flight time, with the ER-2 having longer legs. Given the typical spatial and temporal evolution scales of winter storms, it was necessary to treat each leg as an independent measure. Complex flight schemes such as lawnmower and bowtie patterns, which aim to collect horizontally oriented aerial or volumetric sampling of the storms, generally had limited use during

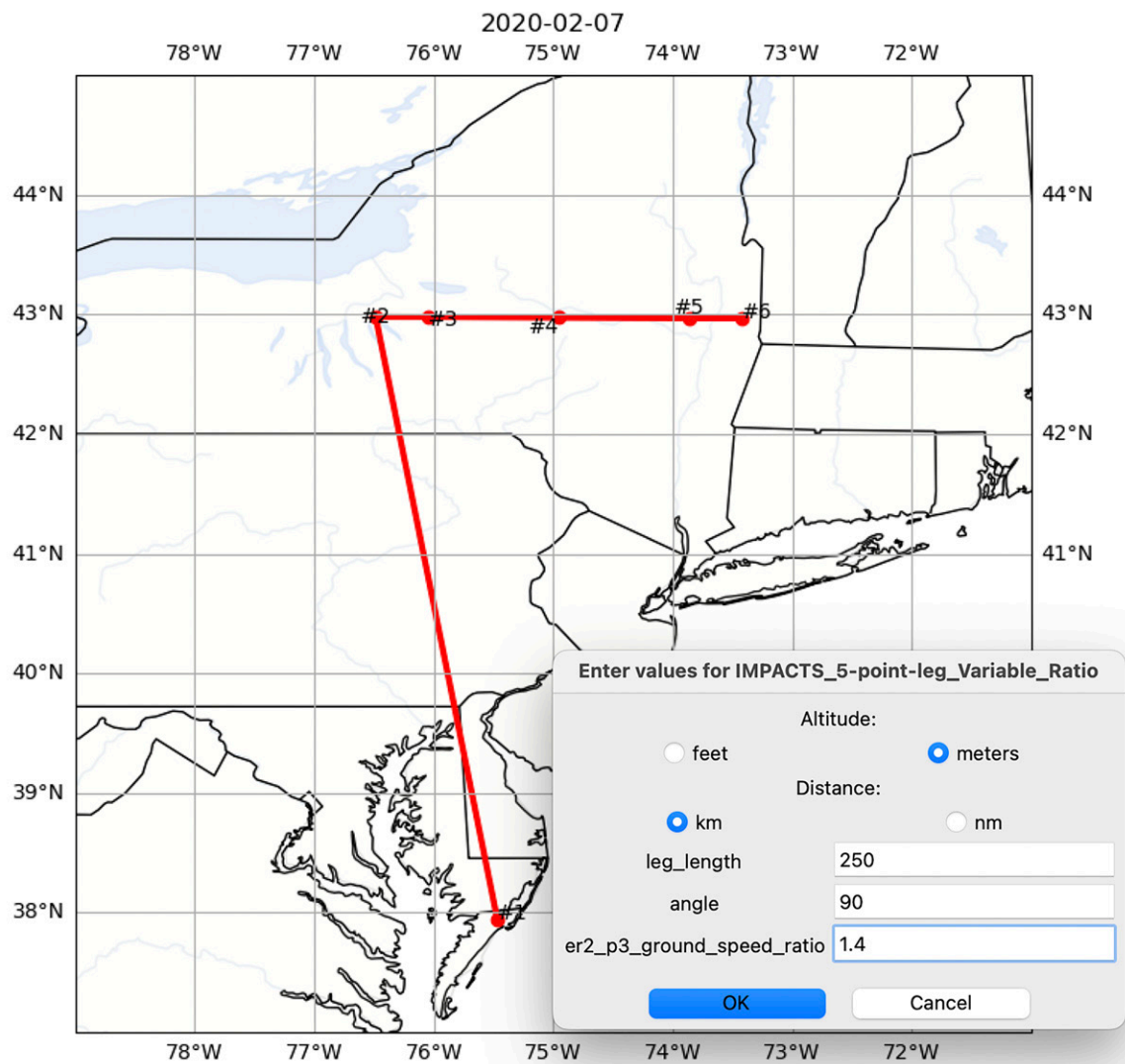


FIG. 4. The five-point line module in the Moving Lines software enabled the IMPACTS mission scientist to enter the leg length and angle (orientation of the line) to create flight plans ahead of each flight (red lines).

IMPACTS since the storms evolve more rapidly than a multileg pattern can be flown. As such, it is inappropriate to make spatial linkages between different flight legs. Lagrangian schemes, which attempt to follow storm features as they advect, were taxing to plan and execute. They required waypoints to be calculated, communicated, manually entered into flight systems, and cleared with ATC in real time based on the storm advection. Waypoint changes can take 15–30 min from calculation to clearance, leaving little margin for error in executing Lagrangian flight patterns. Thus, simple flight patterns have a higher probability of successfully meeting their design goals, and the five-point-leg flight scheme's simplicity provided a benefit in terms of flight planning and execution since different flight leg altitudes or temperatures were flown using a common set of waypoints.

The five-point-line module in the Moving Lines flight planning software allowed mission planners to quickly define all the necessary flight points for both the P-3 and ER-2 by choosing a starting location, a bearing, and a distance (Fig. 4). The software generates all the applicable waypoints for translation into MTS and the Flight Management System of the aircraft. This made transitions between legs easier and quicker to clear with ATC since altitude is the only changing factor. The advection of the storm through the flight path curtain allowed for diversity of sampling with respect to distance and bearing relative to the low pressure center. Since the number of waypoints was small, changing the flight legs during the flight became a simple translation task.

5. Dynamic modifications during flight

Real-time coordination of the aircraft in flight was facilitated by NASA MTS, which enabled real-time tracking of the aircraft, comparison of actually flown tracks to the original flight plans, and simultaneous visualization of geostationary satellite imagery and radar products for in-flight guidance of the aircraft. All ER-2 instruments used Inmarsat to downlink instrument data for “quick look” plots in real time during IMPACTS, which were made available in MTS or other websites accessible to IMPACTS scientists. Dynamic modifications of the flight plan, based on the real-time monitoring using MTS, were coordinated between the lead mission scientist, the ER-2 mission scientist, and the aircraft coordinator on the ground, as well as the P-3 mission scientist onboard, who had direct interaction with P-3 pilots. The lead mission scientist had intimate knowledge of a specific flight plan and the authority to change the flight plan after takeoff.

Communication of changes to the flight plan and the experience of the aircraft coordinator, former ER-2 pilot Jan Nystrom (Fig. 5), were key to successful implementation. The aircraft coordinator used the Nystrom tool (named in honor of him) in MTS (Fig. 6) to compute the coordinates of the start, mid, and end points for the aircraft. The tool provides latitude/longitude of the waypoints in decimal degrees, radial Distance Measuring Equipment arc, and degree minutes simply by dragging the line to a new location with a computer mouse. The aircraft coordinator then passed new waypoints using Internet Relay Chat communicated directly to the ER-2 pilot as well as to the P-3 mission scientist, who then relayed the points to the

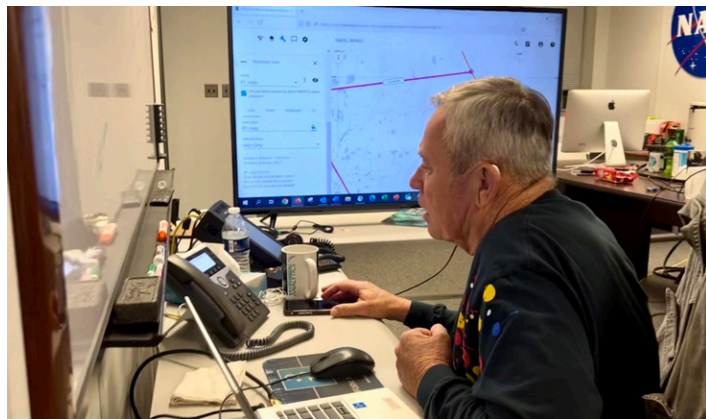


FIG. 5. IMPACTS Aircraft Coordinator Jan Nystrom discusses real-time modifications to a planned IMPACTS flight with the ER-2 pilot during the 2022 deployment.

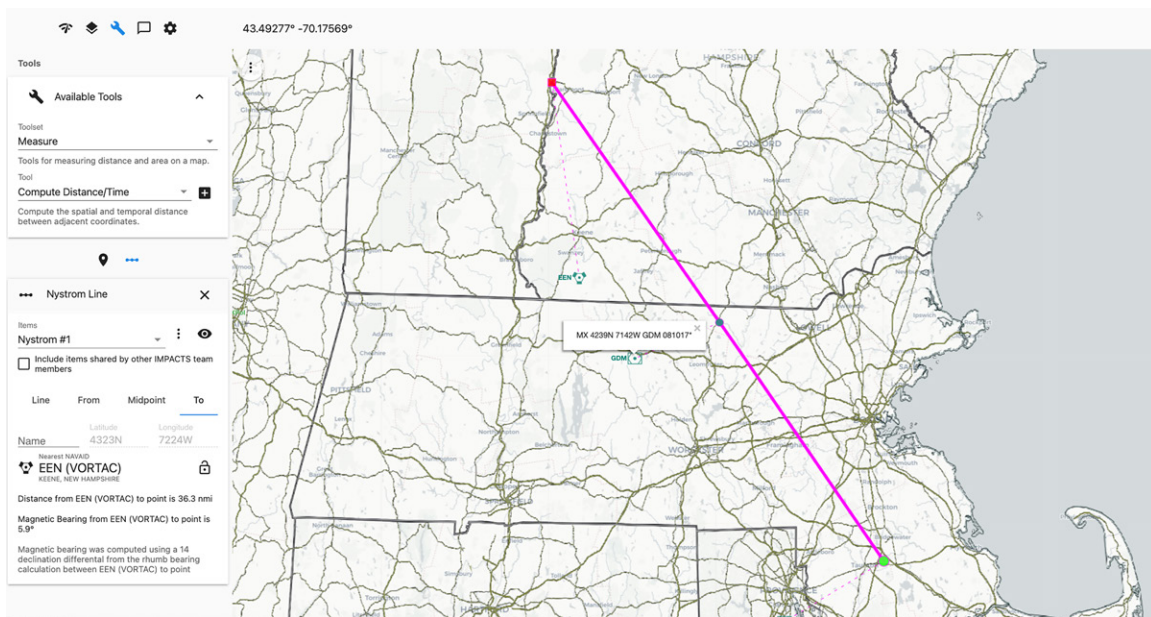


FIG. 6. The Nystrom Line tool (magenta with start, mid, and end points) in the MTS enabled the aircraft coordinator to configure the five-point line and drag the line as needed for dynamic changes. MTS is available to all NASA-funded field campaigns.

P-3 pilots. The flight management system in both aircraft estimated the time at which they would overfly the center point of the next leg in the series considering headwind and planned altitude changes.

When a five-point line is repeated at multiple altitudes, the pilots of the aircraft communicated their estimated time to the next center point to each other via VHF/UHF radios (if within a range of ~500 km) or Internet Relay Chat messages to plan whether to cut short or extend their current leg to set up for well-coordinated segment on the next leg. Typically, the ER-2 performed any necessary deviations for the flight legs because of its high altitude, well above conflicting air traffic, maintaining an area clearance from ATC to fly freely within a certain altitude band without prior permission. The P-3 pilots communicated new waypoints to ATC when necessary, which sometimes resulted in a holding pattern until approved. One advantage of the five-point line is that it required fewer waypoints (3 per aircraft) to be updated, reducing the task load on the flight crews and accelerating communication with ATC.

6. Assessment of IMPACTS collocation success

The IMPACTS dataset is an exceptional collection of winter storm observations from the northeastern and midwestern United States, providing invaluable data that researchers will continue to benefit from for years to come. During 22 storm events, the IMPACTS project collected a specialized dataset comprising more than 21 h of measurements taken within 5 min and less than 4-km horizontal separation between NASA's ER-2 and P-3 aircraft, spanning 106 flight legs. These IMPACTS collocation estimates are determined using the sensor data, ensuring functional instrument's sampling of features of interest (i.e., cloud and precipitation). Collocation statistics cited for CAMEX and ACTIVATE earlier in the paper used the aircraft navigation data, which do not consider sensor functionality or the presence of features. Figure 7 shows a map of the coordinated flight legs. Not all 106 appear on the map, as many of these coordinated legs were flown over the exact same line but at different P-3 altitudes. While most of the coordinated lines are over the Northeast United States, there are several off the mid-Atlantic U.S. coast and over the Midwest. As many as six different storm types were sampled, including Miller Type A and B, Gulf Coast cyclones, Alberta Clippers, cold fronts, and Great Plains cyclones (Zaremba et al. 2024; Lundstrom et al. 2025a,b).

IMPACTS was very successful at collocating the ER-2 and P-3 aircraft, incorporating lessons learned after each deployment to accumulate 21.3 h of collocated data based on HIWRAP. For this paper, a matching routine was developed to identify the nearest 30 HIWRAP radar profiles to the P-3 for every 5 s of flight (Finlon et al. 2022). This radar matching algorithm was modified from the ones described in Chase et al. (2018) and Ding et al. (2020). From there, a Barnes (1964) interpolation procedure was applied to obtain a spatially weighted reflectivity value for each 5-s collocated point. Guided by spatial autocorrelation analysis of the in situ microphysics and remotely sensed measurements among all the coordinated flight legs, 4 km was determined as

the optimal distance threshold based on the autocorrelation index (Moran 1950). Table 3 shows the number of hours IMPACTS collected collocated (2 min and 1 km or 5 min and 4 km) data for each deployment year. During the 2020 deployment, only 3.7 h of collocation within the IMPACTS goal of 5 min and 4 km were achieved, due to the limited number of joint flights and flight plans that did not optimize coordination. The implementation of the five-point line for the 2022 deployment helped the team improve overall collocation to 5.1 h. However, opportunities for collocation were often limited in 2022 due to strong crosswinds at the Pope airfield that were out of limits for a safe ER-2 takeoff or landing. For the 2023 deployment, the implementation of the five-point line module using two ground speed ratio options, the Nystrom line tool in MTS (Fig. 6), better communication between the aircraft pilots in real time, and less weather-related ER-2 delays all led to 12.6 h of collocation, with 5.6 h coordinated to within 2 min and 1 km.

Given that the lidar and radars flown during IMPACTS are sensitive to different portions of the vertical extent of the clouds, collocation with respect to cloud depth is an important factor when combining the in situ and remote sensing datasets. Figure 8 shows the normalized frequency of collocated observations (5 min and 4 km) versus the P-3 altitude with respect to depth below cloud top as observed by the CPL. The 2020 deployment had few (if any) collocations within 2 km of cloud top, but many observations deep (8–10 km) into the clouds, mostly due to concerns about flying near cloud tops that year. In the following deployment years, there was a strong desire to sample a variety of temperature ranges and to sample near cloud top, especially in 2023, to sample the full range of microphysical growth regions, as defined by Bailey and Hallett (2009), i.e., the polycrystalline growth layer in temperatures less than -18°C , dendritic growth layer from -18° to -12°C , the plate growth layer from -12° to -8°C , and the needle growth layer from -8° to -3°C . However, these layers were not always present in every storm or could not

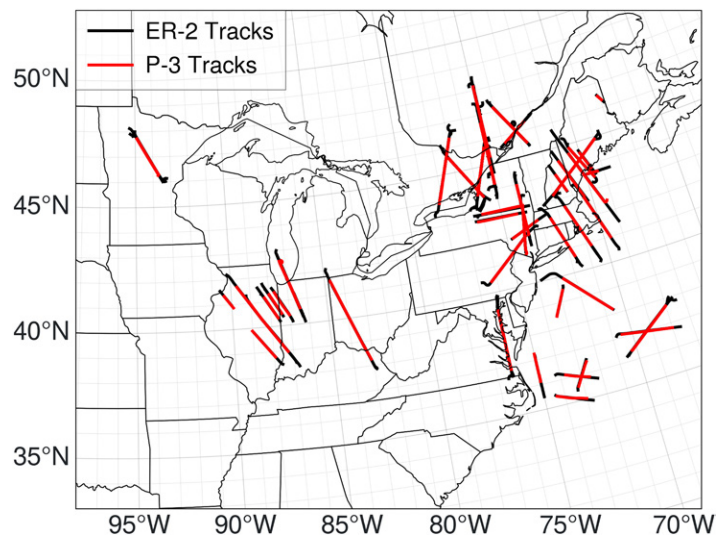


FIG. 7. A map of the coordinated flight legs over all three IMPACTS deployments. The black lines represent the ER-2 flight track, while the red lines represent the P-3 flight track. Many of these tracks are oriented north-northwest to south-southeast to be perpendicular to snowbands and frontal zones. This had the added benefit of reducing cross-track separation error between the two aircraft caused by the amount of great circle correction inherent in flying lines of different lengths. A true north-south-oriented line has no great circle correction, while east-west lines have small persistent corrections dependent on length.

TABLE 3. The IMPACTS collocation sampling hours for each deployment year.

Collocation	2020 (h)	2022 (h)	2023 (h)	Total (h)
2 min and 1 km	1.5	2.0	5.6	9.1
5 min and 4 km	3.7	5.1	12.6	21.3

be sampled for variety of reasons such as being too close to the ground. This resulted in an uneven distribution of sampling by depth below cloud top shown in Fig. 8, especially for the 2022 deployment.

IMPACTS collocations between the in situ sensors and the radar data were more robust than the collocations between the in situ sensors and lidar, given the frequent sampling 2–6 km deep into the clouds. Figure 9 displays the 2D histogram and cumulative distribution functions of all the 5-s collocated observations as a function of aircraft distance and time offset for HIWRAP (Fig. 9a) and CPL (Fig. 9b). The HIWRAP radar and in situ sensors were well collocated in time and space, with 6.28 h of data collocated to within 1 min and 17.15 h collocated to within 1 km, the footprint of the HIWRAP (Ku band) and EXRAD radars. During many flights, the P-3 could be observed as a “skin paint” echo in real-time images of the EXRAD radar reflectivity, as shown in Fig. 10 at 2142 UTC and 4.8-km altitude on 25 January 2023. The wider swath microwave radiometers, especially AMPR and CoSMIR, being sensitive to the lower vertical regions of the clouds, have similar collocation statistics to the radars. However, lidar collocation is not as good as the radars and radiometers due to 1) attenuation of the laser beam $\sim 1\text{--}3$ km into the cloud, 2) limited observations near cloud top in 2020 and 2022, and 3) the narrow footprint diameter (2 m) of CPL. Despite these limitations, IMPACTS still collected 2.83 h of collocated data within a distance offset of less than 1 km and 3.47 h with a time offset of less than 5 min.

7. Enabled science from IMPACTS collocations

Figure 11 illustrates the value of coordinated remote sensing and in situ observations, which enables interpretation of the remote sensing measurements in terms of observed microphysical processes. On 23 January 2023, the aircraft sampled a broad frontal zone over southern Maine. The highlighted flight leg sampled across the front from northwest to southeast as shown in Fig. 11a. During this coordinated leg, the two aircraft flight tracks differed by <220 m in horizontal distance and the aircraft passed over the same point no more than 2 min apart in time from one another, enabling detailed comparisons between the airborne radar and in situ microphysics measurements (Fig. 11e). The frontal zone exhibited a high degree of variability, as

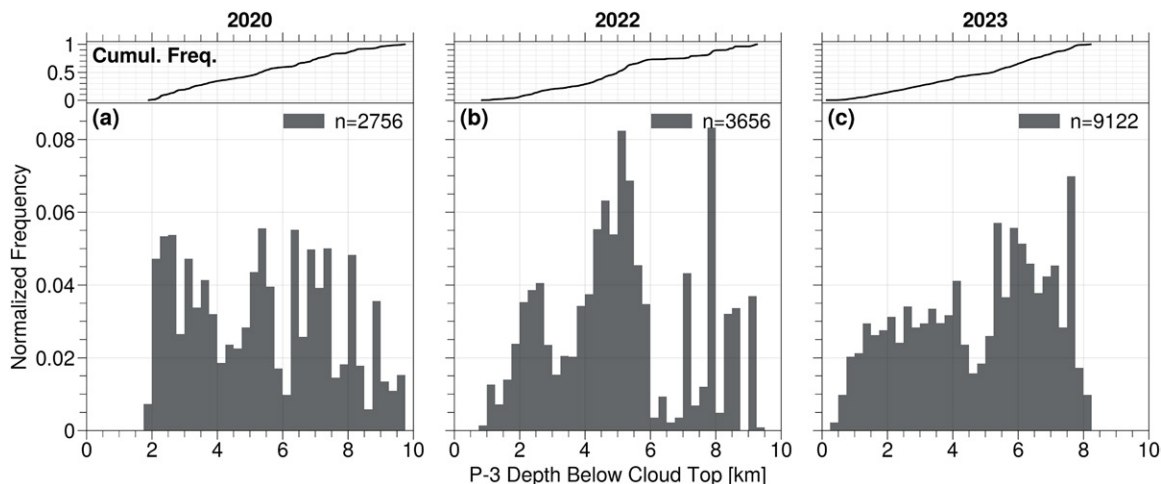


FIG. 8. The normalized frequency of collocations vs the P-3 depth below cloud top for (a) 2020, (b) 2022, and (c) 2023.

evident in the HIWRAP Ku-band and EXRAD reflectivity fields shown in Figs. 11b and 11d.

Using the remote sensing measurements and in situ observations together allows inference of distinct microphysical processes that occurred along this flight leg. At the southern end of the flight leg (44.05°N), a broad region of high reflectivity (>30 dBZ) was observed that appears to be associated with fallstreaks from elevated convection above the front (Fig. 11b). Upward Doppler velocities around 1 m s^{-1} (Fig. 11c) were observed by HIWRAP near cloud top directly above the P-3. EXRAD conical scans of reflectivity show that this high-reflectivity region had a wide horizontal extent at 4 km, near the altitude of the P-3 (Fig. 11d). This region also coincided with high IWC ($0.4\text{--}0.8 \text{ g m}^{-3}$), as calculated using the mass–dimension relationship of Heymsfield et al. (2005), high LWC ($0.02\text{--}0.06 \text{ g m}^{-3}$), and high number concentration of both cloud-sized (from 2DS) and precipitation sized (from HVPS) particles (Figs. 11f,g). Together, these fields paint the picture of the high likelihood of particle growth via both vapor deposition and riming/aggregation beneath cloud top.

In the vicinity of 44.3°N, the P-3 sampled the top of a narrow region of elevated reflectivity (near 30 dBZ, Fig. 11b). The conical scan shows a narrow region of higher reflectivity (near 30 dBZ) surrounded by a broader region of weak reflectivity (<15 dBZ, Fig. 11d). The radial velocities are roughly near zero (Fig. 11c), suggesting weak upward motion. This region contains very high concentrations of small particles (<0.1 mm), low IWC, and low LWC, indicating the lack of supercooled liquid (SLW) droplets within the fall streak (Figs. 11f–h). Substantial LWC (Figs. 11f,h) was observed outside the fallstreak on either side of it, whereas SLW was largely absent within it. In contrast to the other areas characterized by prominent fallstreaks and enhanced ice aloft, such as the one described above, this zone appears to have avoided efficient scavenging of SLW by descending ice, possibly due to the localized nature of the convective fallstreaks or vertical motions that disrupted their descent. The microphysical characteristics support the idea that small-scale vertical motions and gaps between fallstreaks can enable pockets of SLW to persist.

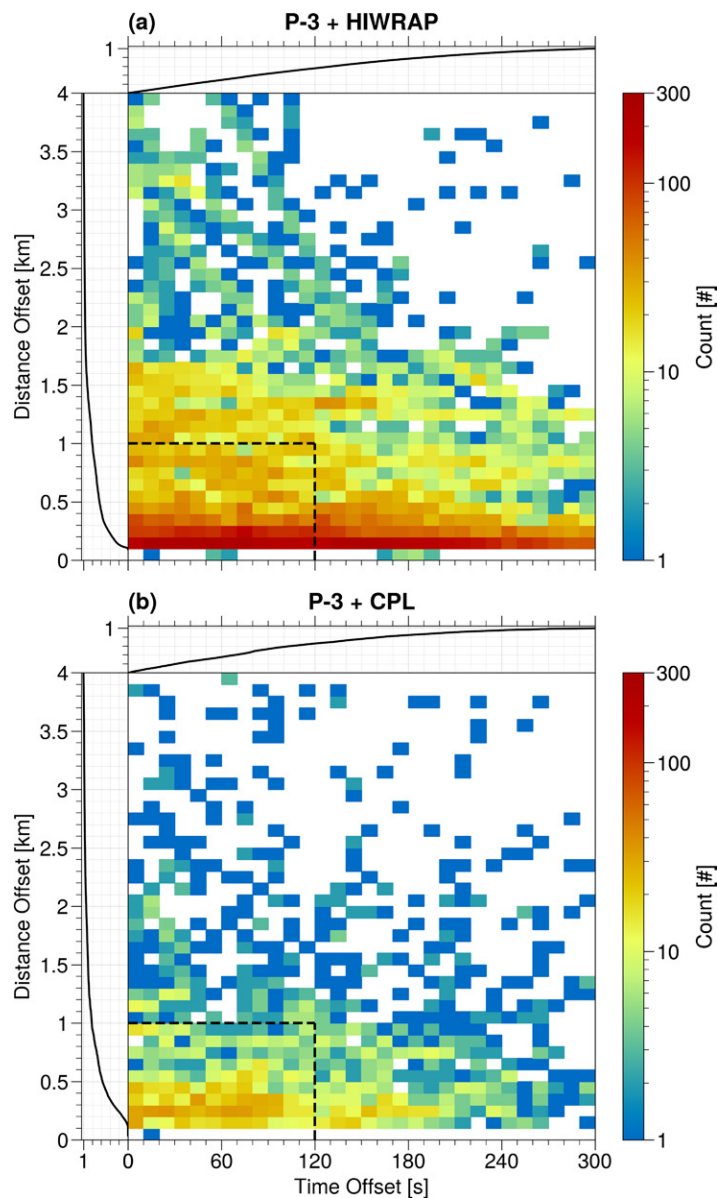


FIG. 9. A 2D histogram of the number of 5-s collocated observations as a function of distance and time offset between (a) the HIWRAP data, (b) the CPL data, and P-3 aircraft's in situ observation. The cumulative distribution functions are provided along each axis side panel. The black dotted box represents the 1-km and 2-min collocation threshold used in Table 3.

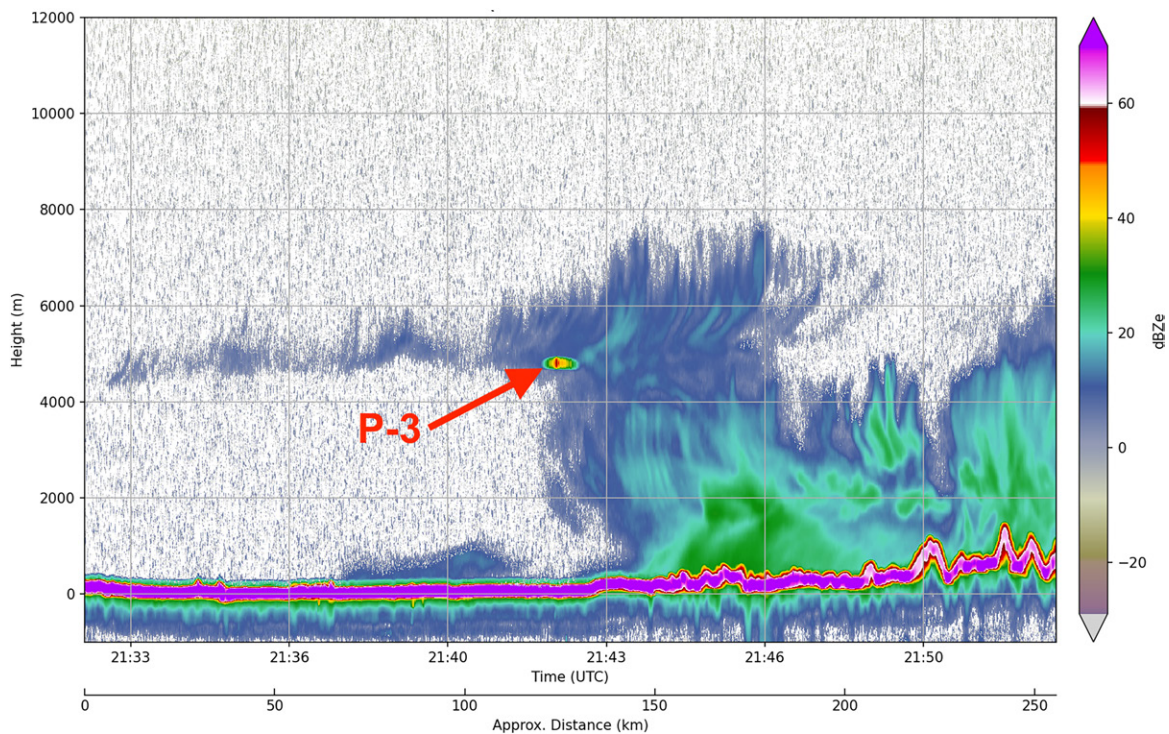


FIG. 10. The EXRAD nadir reflectivity from the IMPACTS flight on 25 Jan 2023. The P-3 aircraft (indicated with red arrow) caused an observed reflectivity of about 40 dBZ (4800-m altitude around 2142 UTC).

8. Concluding remarks, significance, and summary

IMPACTS, a 3-yr NASA field campaign, deployed complementary aircraft—the high-altitude ER-2 with remote sensing instruments flying above storms and the P-3 equipped with in situ probes operating within clouds at various altitudes—to comprehensively study snowband formation, organization, and evolution. By flying the two aircraft in a vertically stacked pattern with a five-point flight leg, IMPACTS was able to collect over 21 h (106 flight legs) of collocated remote sensing and in situ microphysics data for 22 winter storms. This robust collocated dataset, with temporal (5 min or less) and spatial (4 km or less) scales to diagnose particle growth processes within storms, enables scientists to accurately interpret the remote sensing measurements with respect to microphysical processes and environmental conditions, advancing our understanding of clouds and precipitation.

Multiple studies have resulted from the analysis of IMPACTS collocated data. These include in-depth case studies, such as Varcie et al. (2023) documenting the differences in microphysical processes in the stratiform and convective portions of a deepening cyclone, DeLaFrance et al. (2024) illustrating the effects of riming on radar moments and precipitation fallout, Zhang et al. (2025) examining elevated convection and banded precipitation in a broad frontal band, and Han et al. (2025) highlighting the role of supercooled liquid water at cloud top in an intense east coast storm. Studies focusing on microphysical and ice growth processes leveraging the full IMPACTS collocated remote sensing and in situ dataset include Allen et al. (2025) and Heymsfield et al. (2023). Tomkins et al. (2025) utilize multiyear IMPACTS datasets as well as NOAA NWS operational observations to quantify the impact of mesoscale snowbands on surface snowfall rates. Finlon et al. (2022), Zaremba et al. (2024), and Nicholls et al. (2025) demonstrated improvements to remote sensing retrievals of snowfall using the collocated IMPACTS dataset. Furthermore, combining the IMPACTS dataset with numerical weather prediction models enables assessments and improvements to model microphysical schemes (e.g., Colle et al. 2023) as well as the evaluation of the impact of assimilating various types of observations on model analyses and forecasts. While this paper focuses on the direct applications for winter storm and precipitation processes, there are needs

across many different atmospheric composition communities (clouds, aerosols, trace gases, etc.) to understand the connections between spatial structure, microphysical properties, and thermodynamic processes. IMPACTS provides a model for future atmospheric science field campaigns to coordinate remote sensing and in situ aircraft and address these science community needs. Continued investment in collocated airborne platforms capable of collecting radar, lidar, and in situ microphysics remains essential for disentangling the complex vertical and horizontal variability of cloud processes that shape precipitation formation.

Acknowledgments. The IMPACTS project was funded by the NASA Earth Venture Suborbital-3 (EVS-3) program and managed by the Earth System Science Pathfinder (ESSP) Program Office. IMPACTS participation at various universities was funded under NASA Grants 80NSSC19K0338 (UW), 80NSSC19K0354 (NCSSU), 80NSSC19K0452 (PSU), 80NSSC19K0399 (OU), 80NSSC19K0355 (UI), 80NSSC19K0394 (SBU), 80NSSC19K0328 (UND), 80NSSC19K1612 (NCAR), 80NSSC20K1876 (NCAR), 80NSSC19K0397 (NCAR), and 80NSSC20K0729 (CU). It takes many people to successfully operate a field campaign. The authors would like to recognize the many people who made IMPACTS a success, including our aircraft coordinator Jan Nystrom; the navigators Walt Klein, Todd Renfro, Steve Koertge; the ER-2 and P-3 pilots; the aircraft crew; NASA MTS lead Aaron Duley; Vidal Salazar and the ESPO project managers; the forecasters; and all the scientists and students that collected the comprehensive in situ and remote sensing datasets, both on the aircraft and on the ground, enabling this study.

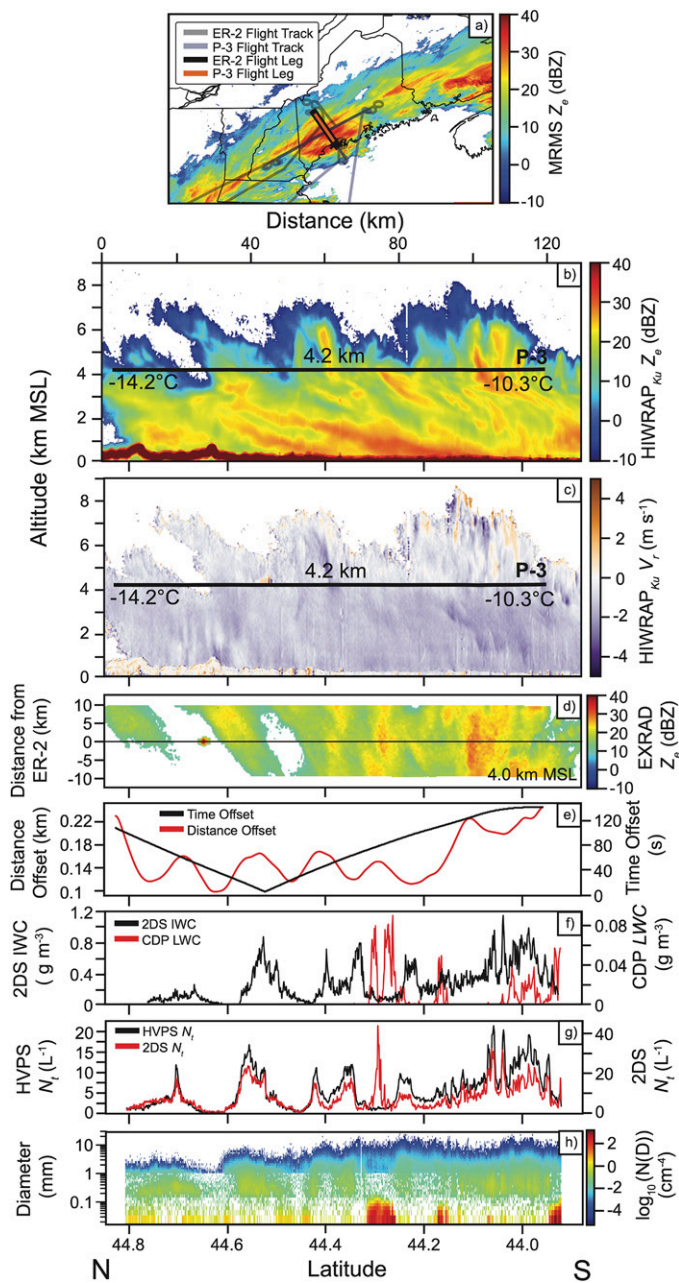


FIG. 11. Data collected between 1637:30 UTC and 1647:30 UTC 23 Jan 2023 by the ER-2 and P-3 aircraft: (a) MRMS composite reflectivity (dBZ; shaded) with flight tracks overlaid for the 23 Jan flight, highlighting the track shown in subsequent panels; (b) HIWRAP Ku-band reflectivity (dBZ; shaded) with P-3 altitude overlaid (black line) and observed temperatures at each end of the track indicated; (c) HIWRAP Ku-band Doppler radial velocity (m s^{-1} ; shaded) with corrections for aircraft motions and horizontal wind applied. P-3 altitude is overlaid as in (b); (d) horizontal distribution of reflectivity from EXRAD conical scans spanning 10 km south and 10 km north of the ER-2 flight track at 4.0 km MSL, gridded at 0.1° latitude and 0.1° longitude following Helms et al. (2020); (e) time (black) and distance (red) offset of the P-3 and ER-2 aircraft during the coordinated leg; (f) total IWC (g m^{-3}) calculated using Heymsfield et al. (2005) from the 2DS probe and total LWC (g m^{-3}) measured by the CDP on the P-3; (g) particle number concentration from the HVPs and 2DS optical array probes; and (h) merged particle size distribution represented as the number distribution function $N(D)$ (cm^{-4} ; shaded).

Data availability statement. Mission scientist reports, weather discussions, and quick-look images from all three IMPACTS deployments are provided in the IMPACTS field catalogs below: 2020: https://catalog.eol.ucar.edu/impacts_2020; 2022: https://catalog.eol.ucar.edu/impacts_2022; 2023: https://catalog.eol.ucar.edu/impacts_2023. All the IMPACTS data can be obtained from the Global Hydrology Resource Center Distributed Active Archive Center at https://ghrc.nsstc.nasa.gov/uso/ds_details/collections/impactsC.html and McMurdie et al. (2019). Python code that matches nadir-pointing data from the CPL, CRS, and HIWRAP to the P-3 location is publicly available (Finlon et al. 2025).

References

- Abdelmonem, A., E. Järvinen, D. Duft, E. Hirst, S. Vogt, T. Leisner, and M. Schnaiter, 2016: PHIPS–HALO: The airborne particle habit imaging and PolarScattering probe—Part 1: Design and operation. *Atmos. Meas. Tech.*, **9**, 3131–3144, <https://doi.org/10.5194/amt-9-3131-2016>.
- Airborne Science Program, 2025: ASP mission tools suite. https://airbornescience.nasa.gov/content/ASP_Mission_Tools_Suite.
- Allen, L. R., S. E. Yuter, D. M. Crowe, M. A. Miller, and K. L. Thornhill, 2025: In-cloud characteristics observed in northeastern and midwestern US non-orographic winter storms with implications for ice particle mass growth and residence time. *Atmos. Chem. Phys.*, **25**, 6679–6701, <https://doi.org/10.5194/acp-25-6679-2025>.
- Amiot, C. G., S. K. Biswas, T. J. Lang, and D. I. Duncan, 2021: Dual-polarization deconvolution and geophysical retrievals from the advanced microwave precipitation radiometer during OLYMPLEX/RADEX. *J. Atmos. Oceanic Technol.*, **38**, 607–628, <https://doi.org/10.1175/JTECH-D-19-0218.1>.
- Bailey, M. P., and J. Hallett, 2009: A comprehensive habit diagram for atmospheric ice crystals: Confirmation from the laboratory, AIRS II, and other field studies. *J. Atmos. Sci.*, **66**, 2888–2899, <https://doi.org/10.1175/2009JAS2883.1>.
- Barnes, S. L., 1964: A technique for maximizing details in numerical weather map analysis. *J. Appl. Meteor.*, **3**, 396–409, [https://doi.org/10.1175/1520-0450\(1964\)003<0396:ATFMDI>2.0.CO;2](https://doi.org/10.1175/1520-0450(1964)003<0396:ATFMDI>2.0.CO;2).
- Blakeslee, R., J. Hall, M. Goodman, P. Parker, L. Freudinger, and M. He, 2007: The real time mission monitor: A situational awareness tool for managing experiment assets. *NASA Science Technology Conf.*, Adelphi, MD, University of Maryland, 5 pp., <https://ntrs.nasa.gov/citations/20070031886>.
- Brown, E. N., C. A. Friehe, and D. H. Lenschow, 1983: The use of pressure fluctuations on the nose of an aircraft for measuring air motion. *J. Appl. Meteor. Climatol.*, **22**, 171–180, [https://doi.org/10.1175/1520-0450\(1983\)022<0171:TUOPFO>2.0.CO;2](https://doi.org/10.1175/1520-0450(1983)022<0171:TUOPFO>2.0.CO;2).
- Chase, R. J., and Coauthors, 2018: Evaluation of triple-frequency radar retrieval of snowfall properties using coincident airborne In situ observations during OLYMPLEX. *Geophys. Res. Lett.*, **45**, 5752–5760, <https://doi.org/10.1029/2018GL077997>.
- Colle, B., P. Yeh, J. Finlon, L. McMurdie, V. McDonald, and A. DeLaFrance, 2023: An investigation of a northeast U.S. cyclone event without well-defined snow banding during IMPACTS. *Mon. Wea. Rev.*, **151**, 2465–2484, <https://doi.org/10.1175/MWR-D-22-0296.1>.
- DeLaFrance, A., L. A. McMurdie, A. K. Rowe, and A. Heymsfield, 2024: Simulated particle evolution within a winter storm: Contributions of riming to radar moments and precipitation fallout. *Atmos. Chem. Phys.*, **24**, 11 191–11 206, <https://doi.org/10.5194/acp-24-11191-2024>.
- Deng, Y., and Coauthors, 2024: Quantifying the spatial inhomogeneity of ice concentration in mixed-phase stratiform cloud using airborne observation. *Atmos. Res.*, **298**, 107153, <https://doi.org/10.1016/j.atmosres.2023.107153>.
- Ding, S., G. M. McFarquhar, S. W. Nesbitt, R. J. Chase, M. R. Poellot, and H. Wang, 2020: Dependence of mass–dimensional relationships on median mass diameter. *Atmosphere*, **11**, 756, <https://doi.org/10.3390/atmos11070756>.
- Finlon, J., V. McDonald, L. McMurdie, V. Garcia, A. DeLaFrance, and N. Maherndl, 2025: IMPACTS tools version v1.0.0. Zenodo, <https://doi.org/10.5281/zenodo.15310598>.
- Finlon, J. A., G. M. McFarquhar, R. M. Rauber, D. M. Plummer, B. F. Jewett, D. Leon, and K. R. Knupp, 2016: A comparison of X-band polarization parameters with in situ microphysical measurements in the comma head of two winter cyclones. *J. Atmos. Oceanic Technol.*, **55**, 2549–2574, <https://doi.org/10.1175/JAMC-D-16-0059.1>.
- , L. A. McMurdie, and R. J. Chase, 2022: Investigation of microphysical properties within regions of enhanced dual-frequency ratio during the IMPACTS field campaign. *J. Atmos. Sci.*, **79**, 2773–2795, <https://doi.org/10.1175/JAS-D-21-0311.1>.
- Ganetis, S. A., and B. A. Colle, 2015: The thermodynamic and microphysical evolution of an intense snowband during the northeast U.S. blizzard of 8–9 February 2013. *Mon. Wea. Rev.*, **143**, 4104–4125, <https://doi.org/10.1175/MWR-D-14-00407.1>.
- Greco, M., W. Olson, S. Munchak, S. Ringerud, L. Liao, Z. Haddad, B. Kelley, and S. McLaughlin, 2016: The GPM combined algorithm. *J. Atmos. Oceanic Technol.*, **33**, 2225–2245, <https://doi.org/10.1175/JTECH-D-16-0019.1>.
- , L. Tian, G. M. Heymsfield, A. Tokay, W. S. Olson, A. J. Heymsfield, and A. Bansemmer, 2018: Nonparametric methodology to estimate precipitating ice from multiple-frequency radar reflectivity observations. *J. Appl. Meteor. Climatol.*, **57**, 2605–2622, <https://doi.org/10.1175/JAMC-D-18-0036.1>.
- Greybush, S. J., S. Saslo, and R. Grumm, 2017: Assessing the ensemble predictability of precipitation forecasts for the January 2015 and 2016 East Coast winter storms. *Wea. Forecasting*, **32**, 1057–1078, <https://doi.org/10.1175/WAF-D-16-0153.1>.
- Han, M., S. A. Braun, W. S. Olson, P. O. G. Persson, and J.-W. Bao, 2010: Application of TRMM PR and TMI measurements to assess cloud microphysical schemes in the MM5 for a winter storm. *J. Appl. Meteor.*, **49**, 1129–1148, <https://doi.org/10.1175/2010JAMC2327.1>.
- , —, T. Matsui, and C. Williams, 2013: Evaluation of cloud microphysics schemes in simulations of a winter storm using radar and radiometer measurements. *J. Geophys. Res. Atmos.*, **118**, 1401–1419, <https://doi.org/10.1002/jgrd.50115>.
- , —, —, and T. Iguchi, 2018: Comparisons of bin and bulk microphysics schemes in simulations of topographic winter precipitation with radar and radiometer measurements. *Quart. J. Roy. Meteor. Soc.*, **144**, 1926–1946, <https://doi.org/10.1002/qj.3393>.
- , —, T. Lang, M. L. Walker McLinden, G. M. Heymsfield, L. Li, and K. L. Thornhill, 2025: Supercooled liquid water at the top of a snow-producing nimbostratus cloud and its association with gravity wave breaking and turbulence: An IMPACTS case study. *J. Geophys. Res. Atmos.*, **130**, e2024JD041795, <https://doi.org/10.1029/2024JD041795>.
- Hashino, T., 2007: Explicit simulation of ice particle habits in a Numerical Weather Prediction Model. Ph.D. dissertation, University of Wisconsin–Madison, 313 pp., <https://www.aos.wisc.edu/uwaosjournal/Volume4/theses/Hashino.pdf>.
- Helms, C. N., M. L. Walker McLinden, G. M. Heymsfield, and S. R. Guimond, 2020: Reducing errors in velocity–azimuth display (VAD) wind and deformation retrievals from airborne Doppler radars in convective environments. *J. Atmos. Oceanic Technol.*, **37**, 2251–2266, <https://doi.org/10.1175/JTECH-D-20-0034.1>.
- Heymsfield, A. J., Z. Wang, and S. Matrosov, 2005: Improved radar ice water content retrieval algorithms using coincident microphysical and radar measurements. *J. Appl. Meteor.*, **44**, 1391–1412, <https://doi.org/10.1175/JAM2282.1>.
- , C. Schmitt, C.-C.-J. Chen, A. Bansemmer, A. Gettelman, P. R. Field, and C. Liu, 2020: Contributions of the liquid and ice phases to global surface precipitation: Observations and global climate modeling. *J. Atmos. Sci.*, **77**, 2629–2648, <https://doi.org/10.1175/JAS-D-19-0352.1>.
- Heymsfield, G. M., L. Li, M. L. Walker McLinden, L. Liao, C. N. Helms, and S. Guimond, 2023: NASA high altitude airborne weather radars. *Advances in Weather Radar. Volume 1: Precipitation Sensing Platforms*, Institution of Engineering and Technology, 231–282, https://doi.org/10.1049/SBRA557F_ch7.
- Houze, R. A., and Coauthors, 2017: The Olympic Mountains Experiment (OLYMPLEX). *Bull. Amer. Meteor. Soc.*, **98**, 2167–2188, <https://doi.org/10.1175/BAMS-D-16-0182.1>.
- Kakar, R., M. Goodman, R. Hood, and A. Guillory, 2006: Overview of the Convection and Moisture Experiment (CAMEX). *J. Atmos. Sci.*, **63**, 5–18, <https://doi.org/10.1175/JAS3607.1>.
- Kroodsma, R. A., M. A. Fritts, J. F. Lucey, M. R. Schwaller, T. J. Ames, C. M. Cooke, and L. M. Hilliard, 2019: CoSMIR performance during the GPM OLYMPLEX

- campaign. *IEEE Trans. Geosci. Remote Sens.*, **57**, 6397–6407, <https://doi.org/10.1109/TGRS.2019.2906039>.
- LeBlanc, S., 2018: samuelleblanc/fp:Moving lines:NASA airborne research flight planning tool release (v1.21). Zenodo, <https://doi.org/10.5281/zenodo.1478126>.
- Li, L., and Coauthors, 2016: The NASA high-altitude imaging wind and rain airborne profiler. *IEEE Trans. Geosci. Remote Sens.*, **54**, 298–310, <https://doi.org/10.1109/TGRS.2015.2456501>.
- Liu, Y., and I. S. Adams, 2025: Tomographic reconstruction algorithms for retrieving two-dimensional ice cloud microphysical parameters using along-track (sub)millimeter-wave radiometer observations. *Atmos. Meas. Tech.*, **18**, 1659–1674, <https://doi.org/10.5194/amt-18-1659-2025>.
- Lundstrom, K. H., R. M. Rauber, G. Heymsfield, M. Walker-McLinden, and L. McMurdie, 2025a: Manifestation of elevated convection within wintertime extratropical cyclones during IMPACTS. Part I: Analysis of elevated potential instability. *J. Atmos. Sci.*, **82**, 955–978, <https://doi.org/10.1175/JAS-D-24-0198.1>.
- , ———, M. Walker-McLinden, J. Finlon, G. Heymsfield, and L. McMurdie, 2025b: Manifestation of elevated convection within wintertime extratropical cyclones during IMPACTS. Part II: Hydrometeor vertical motions within and outside of elevated potentially unstable layers. *J. Atmos. Sci.*, **82**, 979–998, <https://doi.org/10.1175/JAS-D-24-0199.1>.
- Maherndl, N., M. Moser, I. Schirmacher, A. Bansemer, J. Lucke, C. Voigt, and M. Maahn, 2024: How does riming influence the observed spatial variability of ice water in mixed-phase clouds? *Atmos. Chem. Phys.*, **24**, 13 935–13 960, <https://doi.org/10.5194/acp-24-13935-2024>.
- McGill, M., D. Hlavka, W. Hart, V. S. Scott, J. Spinhirne, and B. Schmid, 2002: Cloud physics lidar: Instrument description and initial measurement results. *Appl. Opt.*, **41**, 3725–3734, <https://doi.org/10.1364/ao.41.003725>.
- McMurdie, L. A., G. Heymsfield, J. E. Yorks, and S. A. Braun, 2019: Investigation of Microphysics and Precipitation for Atlantic Coast-Threatening Snowstorms (IMPACTS) Collection. NASA EOSDIS Global Hydrology Resource Center Distributed Active Archive Center, Huntsville, Alabama, <https://doi.org/10.5067/IMPACTS/DATA101>.
- McMurdie, L. A., and Coauthors, 2022: Chasing snowstorms: The Investigation of Microphysics and Precipitation for Atlantic Coast-Threatening Snowstorms (IMPACTS) campaign. *Bull. Amer. Meteor. Soc.*, **103**, E1243–E1269, <https://doi.org/10.1175/BAMS-D-20-0246.1>.
- Moran, P., 1950: Notes on continuous stochastic phenomena. *Biometrika*, **37**, 17–23, <https://doi.org/10.1093/biomet/37.1-2.17>.
- Nicholls, S. D., A. Heymsfield, G. M. Heymsfield, J. E. Yorks, A. Bansemer, C. Aubry, M. Deng, and J. Delanoë, 2025: Evaluation of physical microphysical property retrieval algorithms during the 2020 IMPACTS field campaign. *J. Atmos. Oceanic Technol.*, **42**, 167–186, <https://doi.org/10.1175/JTECH-D-23-0106.1>.
- Plummer, D. M., G. M. McFarquhar, R. M. Rauber, B. F. Jewett, and D. Leon, 2014: Structure and statistical analysis of the microphysical properties of generating cells in the comma head region of continental winter cyclones. *J. Atmos. Sci.*, **71**, 4181–4203, <https://doi.org/10.1175/JAS-D-14-0100.1>.
- , ———, ———, ———, and ———, 2015: Microphysical structure of fall streaks in stratiform areas within winter cyclones. *J. Atmos. Sci.*, **72**, 2465–2483, <https://doi.org/10.1175/JAS-D-14-0354.1>.
- Podolske, J. R., G. W. Sachse, and G. S. Diskin, 2003: Calibration and data retrieval algorithms for the NASA Langley/Ames diode laser hygrometer for the NASA Transport and Chemical Evolution over the Pacific (TRACE-P) mission. *J. Geophys. Res.*, **108**, 8792, <https://doi.org/10.1029/2002JD003156>.
- Putnam, B., M. Xue, Y. Jung, G. Zhang, and F. Kong, 2017: Simulation of polarimetric radar variables from 2013 CAPS spring experiment storm-scale ensemble forecasts and evaluation of microphysics schemes. *Mon. Wea. Rev.*, **145**, 49–73, <https://doi.org/10.1175/MWR-D-15-0415.1>.
- Ralph, M., and Coauthors, 2005: Improving short term (0–48 hour) cool season quantitative precipitation forecasting: Recommendations from a USWRP workshop. *Bull. Amer. Meteor. Soc.*, **86**, 1619–1632.
- Redemann, J., and Coauthors, 2021: An overview of the ORACLES (ObseRvations of aerosols above clouds and their interactions) project: Aerosol–cloud–radiation interactions in the southeast Atlantic basin. *Atmos. Chem. Phys.*, **21**, 1507–1563, <https://doi.org/10.5194/acp-21-1507-2021>.
- Richter, A., and T. J. Lang, 2024: An airborne multifrequency microwave analysis of precipitation within two winter cyclones. *Mon. Wea. Rev.*, **152**, 725–743, <https://doi.org/10.1175/MWR-D-23-0104.1>.
- Schlosser, J. S., and Coauthors, 2024: Maximizing the volume of collocated data from two coordinated suborbital platforms. *J. Atmos. Oceanic Technol.*, **41**, 189–201, <https://doi.org/10.1175/JTECH-D-23-0001.1>.
- Schnaiter, M., E. Järvinen, A. Abdelmonem, and T. Leisner, 2018: PHIPS-HALO: The airborne particle habit imaging and polar scattering probe—Part 2: Characterization and first results. *Atmos. Meas. Tech.*, **11**, 341–357, <https://doi.org/10.5194/amt-11-341-2018>.
- Schultz, C. J., and Coauthors, 2021: Remote sensing of electric fields observed within winter precipitation during the 2020 Investigation of Microphysics and Precipitation for Atlantic Coast-Threatening Snowstorms (IMPACTS) field campaign. *J. Geophys. Res. Atmos.*, **126**, e2021JD034704, <https://doi.org/10.1029/2021JD034704>.
- Stark, D., B. A. Colle, and S. E. Yuter, 2013: Observed microphysical evolution for two East Coast winter storms and the associated snow bands. *Mon. Wea. Rev.*, **141**, 2037–2057, <https://doi.org/10.1175/MWR-D-12-00276.1>.
- Tomkins, L. M., S. E. Yuter, M. A. Miller, M. Oue, and C. N. Helms, 2025: Synthesis of surface snowfall rates and radar-observed storm structures in 10+ years of northeastern US winter storms. *Atmos. Chem. Phys.*, **25**, 9999–10 026, <https://doi.org/10.5194/acp-25-9999-2025>.
- Twohy, C. H., A. J. Schanot, and W. A. Cooper, 1997: Measurement of condensed water content in liquid and ice clouds using an airborne counterflow virtual impactor. *J. Atmos. Oceanic Technol.*, **14**, 197–202, [https://doi.org/10.1175/1520-0426\(1997\)014<0197:MOCWCI>2.0.CO;2](https://doi.org/10.1175/1520-0426(1997)014<0197:MOCWCI>2.0.CO;2).
- Varcie, M. M., and Coauthors, 2023: Precipitation growth processes in the comma-head region of the 7 February 2020 northeast snowstorm: Results from IMPACTS. *J. Atmos. Sci.*, **80**, 3–29, <https://doi.org/10.1175/JAS-D-22-0118.1>.
- Waitz, F., M. Schnaiter, T. Leisner, and E. Järvinen, 2021: PHIPS-HALO: The airborne particle habit imaging and polar scattering probe—Part 3: Single-particle phase discrimination and particle size distribution based on the angular-scattering function. *Atmos. Meas. Tech.*, **14**, 3049–3070, <https://doi.org/10.5194/amt-14-3049-2021>.
- Walker McLinden, M. L., L. Li, G. M. Heymsfield, M. Coon, and A. Emory, 2021: The NASA GSFC 94-GHz airborne solid-state Cloud Radar System (CRS). *J. Atmos. Oceanic Technol.*, **38**, 1001–1017, <https://doi.org/10.1175/JTECH-D-20-0127.1>.
- Yorks, J. E., D. L. Hlavka, M. A. Vaughan, M. J. McGill, W. D. Hart, S. Rodier, and R. Kuehn, 2011a: Airborne validation of cirrus cloud properties derived from CALIPSO lidar measurements: Spatial properties. *J. Geophys. Res.*, **116**, D19207, <https://doi.org/10.1029/2011JD015942>.
- , M. McGill, D. Hlavka, and W. Hart, 2011b: Statistics of cloud optical properties from airborne lidar measurements. *J. Atmos. Oceanic Technol.*, **28**, 869–883, <https://doi.org/10.1175/2011JTECHA1507.1>.
- Zaremba, T., and Coauthors, 2024: Cloud-top phase characterization of extratropical cyclones over the northeast and midwest United States: Results from IMPACTS. *J. Atmos. Sci.*, **81**, 341–361, <https://doi.org/10.1175/JAS-D-23-0123.1>.
- Zhang, F., C. Snyder, and R. Rotunno, 2002: Mesoscale predictability of the “surprise” snowstorm of 24–25 January 2000. *Mon. Wea. Rev.*, **130**, 1617–1632, [https://doi.org/10.1175/1520-0493\(2002\)130<1617:MPOTSS>2.0.CO;2](https://doi.org/10.1175/1520-0493(2002)130<1617:MPOTSS>2.0.CO;2).
- Zhang, S., and Coauthors, 2025: Mesoscale and microphysical characteristics of elevated convection and banded precipitation over an Arctic cold front: A case study from IMPACTS. *J. Atmos. Sci.*, **82**, 1113–1135, <https://doi.org/10.1175/JAS-D-24-0177.1>.